Estimating Lava Volume by Precision Combination of Multiple Baseline Spaceborne and Airborne Interferometric Synthetic Aperture Radar: The 1997 Eruption of Okmok Volcano, Alaska

Zhong Lu, *Member, IEEE*, Eric Fielding, Matthew R. Patrick, and Charles M. Trautwein

***Abstract*—Interferometric synthetic aperture radar (InSAR) techniques are used to calculate the volume of extrusion at Okmok volcano, Alaska by constructing precise digital elevation models (DEMs) that represent volcano topography before and after the 1997 eruption. The posteruption DEM is generated using airborne topographic synthetic aperture radar (TOPSAR) data where a three-dimensional affine transformation is used to account for the misalignments between different DEM patches. The preeruption DEM is produced using repeat-pass European Remote Sensing satellite data; multiple interferograms are combined to reduce errors due to atmospheric variations, and deformation rates are estimated independently and removed from the interferograms used for DEM generation. The extrusive flow volume associated with the 1997 eruption of Okmok volcano is 0.154 ± 0.025 km^3. The thickest portion is approximately 50 m, although field measurements of the flow margin's height do not exceed 20 m. The *in situ* measurements at lava edges are not representative of the total thickness, and precise DEM data are absolutely essential to calculate eruption volume based on lava thickness estimations. This study is an example that demonstrates how InSAR will play a significant role in studying volcanoes in remote areas.**

***Index Terms*—Interferometry, remote sensing, surfaces, synthetic aperture radar, terrain mapping.**

I. Introduction

ESTIMATING eruption volume is a critical component of volcanology. Accurate mapping of the erupted material is valuable for constraining magma supply and understanding the magma plumbing system [1]–[4]. For some volcanic eruptions, a major part of the eruption volume is extruded as lava flows on the surface. Calculating lava flow volume requires accurate mapping of the pre- and posteruption digital elevation models (DEMs) [4]–[7]. In the absence of high-precision DEMs, the eruptive volume is often calculated by multiplying the areal extent of new lava and the average thickness of the extruded material, estimated at several points along the lava edges [5]–[7]. Ground access to lava flows in remote areas is often difficult; therefore, accurate calculation of the eruptive volume has been generally not feasible. For Alaskan volcanoes, the remote locations, difficult logistics, and persistent cloud cover hinder the precise mapping of high-resolution DEMs obtained using optical photogrammetry or light detection and ranging (LIDAR) techniques [8], [9].

Interferometric synthetic aperture radar (InSAR) has proven capable of mapping ground deformation with centimeter-scale precision and producing accurate DEMs with several meters accuracy [10]–[14]. An InSAR image is obtained by interfering synthetic aperture radar (SAR) signals from two spatially or temporally separated antennas. The two antennas are always spatially separated, but only with repeat-pass interferometry are they also temporally separated. The spatial separation of the two antennas is called the baseline. The two antennas may be mounted on a single platform for single-pass (simultaneous) interferometry, the usual implementation for aircraft systems such as topographic SAR (TOPSAR) [15] and the spaceborne Shuttle Radar Topography Mission [16]. Alternatively, InSAR data can be acquired by utilizing a single antenna on an airborne or spaceborne platform (or identical SAR systems) in nearly identical repeating orbits for repeat-pass interferometry [10], [12], [13], [17]. For the latter case, even though the antennas do not illuminate the same area at the same time, the two sets of signals recorded during the two passes will be highly correlated if the scattering properties of the ground surface are unchanged between viewings. This is the typical implementation for spaceborne sensors such as the European Remote Sensing Satellites (ERS-1, operating from 1991 to 2000, and ERS-2, operating from 1995 to present), Canadian Radar Satellite (Radarsat-1, operating from 1995 to present), Japanese Earth Resource Satellite (JERS-1, operating from 1992 to 1998), and the European Environmental Satellite (Envisat, launched in March 2002 and beginning operation), which operate at wavelengths ranging from a few centimeters (C-band) to tens of centimeters (L-band). Note that ERS-1 and ERS-2 were identical SAR systems, which allows interferometry between them.

Manuscript received March 19, 2002; revised October 14, 2002. ERS-1/ERS-2 SAR images are copyright 1993 and 1995 ESA and provided by the Alaska SAR Facility (ASF). This work was supported by the National Aeronautics and Space Administration (NASA) under Contract NRA-99-OES-10 RADARSAT-0025–0056 and in part by U.S. Geological Survey under Contract O3CRCN0001 and Contract 1434-CR-97-CN-40274. Part of this work was performed at the Jet Propulsion Laboratory, California Institute of Technology under contract with NASA.

Z. Lu is with the U.S. Geological Survey, EROS Data Center, SAIC, Sioux Falls, SD 57198 USA (e-mail: lu@usgs.gov).

C. M. Trautwein is with the U.S. Geological Survey, EROS Data Center, Sioux Falls, SD 57198 USA (e-mail: trautwein@usgs.gov).

E. Fielding is with the Jet Propulsion Laboratory, California Institute of Technology, Pasadena, CA 91109 USA (e-mail: Eric.Fielding@jpl.nasa.gov).

M. R. Patrick is with the Alaska Volcano Observatory, Geophysical Institute, University of Alaska, Fairbanks, AK 99775 USA (e-mail: patrick@gi.alaska.edu).

Digital Object Identifier 10.1109/TGRS.2003.811553

In this paper, we use InSAR-derived DEMs to estimate the lava flow volume of the 1997 eruption of Okmok volcano, Alaska (Fig. 1). Okmok volcano, a broad shield topped with a 10-km-wide caldera, occupies most of the northeastern end of Umnak Island, Alaska (Fig. 1). The caldera was formed between eruptions about 8000 and 2000 years ago [18]. Eruptions in this century occurred in 1931, 1936, 1938, 1943, 1945, 1958, 1960, 1981, 1983, 1986, 1988, and 1997. All historic eruptions of Okmok originated from Cone A, a cinder cone located on the southern edge of the caldera floor. Abundant ash emissions and mafic lava flows originating from Cone A have crossed the caldera floor. The latest eruption of Okmok volcano began in early February 1997 and ended in late April 1997. The eruption was a moderate Hawaiian to Strombolian type with an ash plume reaching to 10 000 m. The 1997 flow is generally similar to the other historical flows; all are basaltic aa lava and traveled at least a few kilometers from cone A. The 1997 flow is larger in area than the 1945, but quite a bit smaller in area than the 1958. The amount of pyroclastic material during the 1997 eruption is negligible. ERS-1/-2 InSAR data were used to map the preeruptive, coeruptive, and posteruptive deformation [19]–[21]. The authors measured about 140 cm of subsidence associated with the 1997 eruption of Okmok volcano. This subsidence occurred during an interval beginning 16 months prior to the eruption and ending five months after the eruption. The subsidence was preceded by about 18 cm of uplift between 1992 and 1995, centered in the same location as the coeruptive subsidence source, and was followed by about 10 cm of uplift between September 1997 and 1998 [20], [21]. Suitable SAR data were not available to measure any possible deformation from 1995 to the time before the eruption.

To estimate the eruption volume from the 1997 eruption at Okmok volcano, we use two precise DEMs best describing the volcano topography before and after the 1997 eruption. The data processing flow is shown in Fig. 2. The posteruption DEM is produced using airborne single-pass InSAR system (National Aeronautics and Space Administration (NASA) Jet Propulsion Laboratory (JPL) TOPSAR) whereas the preeruption DEM is generated using spaceborne (ERS-1/ERS-2) repeat-pass InSAR data. We first discuss the background of InSAR DEM generation. Then we present the procedure for producing the DEM mosaic from TOPSAR data and the procedure for generating the DEM from repeat-pass ERS-1/ERS-2 data. We describe the TOPSAR data processing for the posteruption DEM before the ERS-1/ERS-2 InSAR processing for the preeruption DEM because the TOPSAR DEM is used in producing the preeruption DEM. Finally, eruption volume associated with the 1997 eruption of Okmok volcano is calculated.

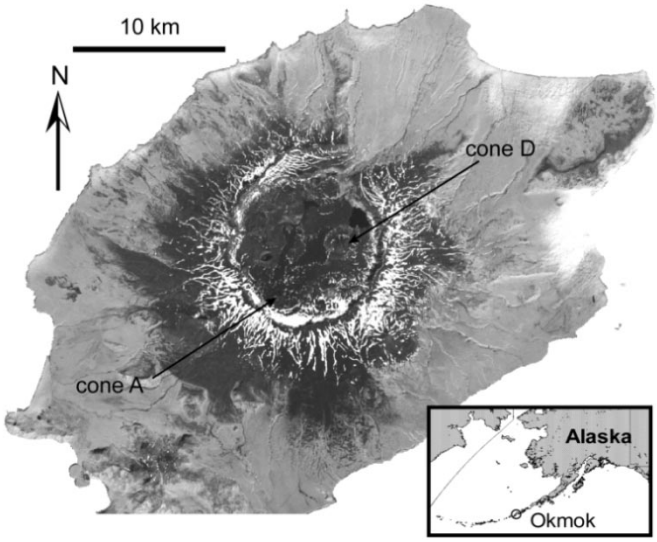

Fig. 1. Terrain-corrected, georeferenced Landsat-7 enhanced Thematic Mapper Plus image (band 8) of Okmok volcano. The image was acquired on August 18, 2000. The location of Okmok volcano relative to the Alaska and the Aleutian arc is shown in the inset.

II. Background of InSAR DEM Generation

The theory of DEM generation by the means of InSAR has been addressed in many papers [10]–[14], [22]. Here, we just review the particular issues affecting DEM accuracy.

First, a major error source in repeat-pass InSAR DEM generation is the baseline uncertainty due to inaccurate determination of SAR antenna positions. Errors in this value propagate into very large systematic errors of terrain height. For this study, the precision orbit data product (PRC) delivered by the German Processing and Archiving Facility (D-PAF) for ERS-1/ERS-2 satellites [23] is used for the baseline vector estimation. PRC state vectors are given at 30-s intervals. The accuracy of the PRC position vectors is approximately 30 cm along-track and 8 cm cross-track [23]. The ERS interferometric baseline estimation is further improved by using ground points with known elevation [24]. For the TOPSAR data, due to precision navigation and orientation systems on the aircraft and fixed baseline length, effective baselines (including the effects of electronic delays and antenna phase centers) can be calculated from calibration of the TOPSAR system [15].

Second, error in phase measurement also contributes to the topographic error because the phase of radar signal is used to estimate elevation. The random phase error is generally caused by thermal noise in the SAR system and by decorrelation or incoherence that is in turn caused by volume scattering for both simultaneous and repeat-pass InSAR and environmental change of the imaged surface for repeat-pass InSAR. The surface changes tend to accumulate with time, so longer time interval between passes of an InSAR pair results in poorer coherence [25]. The elevation error due to a given phase error is inversely proportional to the perpendicular component of baseline length; longer baselines are necessary for high-precision DEMs. Unless the volume scattering is negligible and an ideal spectrum filtering is applied [26], [27], however, longer baselines cause geometric decorrelation. This results in an increase in the phase error and consequently the elevation error. Therefore, for the preeruption DEM, we choose interferograms with the largest available baseline within the limits of correlation [28], [29].

Third, a critical error source in DEMs derived from repeat-pass InSAR is due to atmospheric delay anomalies caused by small variations in the index of refraction along the line of propagation [29], [30]. Changes in the total electron content of the ionosphere and water vapor content in the troposphere will result in variations

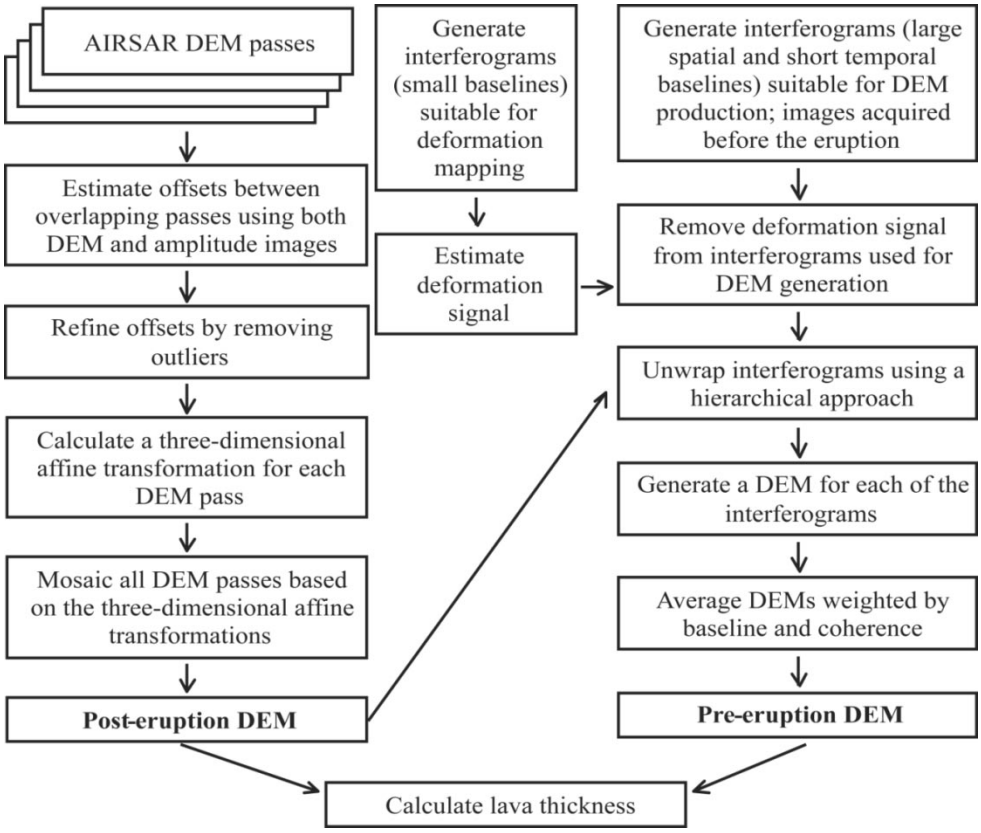

Fig. 2. Block diagram of the data processing flow.

of phase of signals, which will introduce errors in the observed interferogram. Height errors due to atmospheric anomalies are typically not as large as those resulting from baseline errors, but they are less systematic [29], [30]. To produce an accurate DEM from ERS data, it is therefore required 1) to choose interferograms with relatively long baselines as the effect of atmospheric anomalies on DEM heights is inversely proportional to baseline length and 2) to average multiple interferograms to reduce the atmospheric effects [29].

Finally, we must take into account any possible surface deformation due to tectonic, volcanic, or other loading sources over the time interval spanned by repeat-pass interferograms [31]. Therefore, interferograms with shorter temporal separation are preferred for generating DEMs. The ERS-1/ERS-2 Tandem data meet this requirement in most cases. During the ERS-1/ERS-2 Tandem mission phase, interferometric pairs were acquired by adjusting the ERS-1 and ERS-2 orbits, each of which repeat every 35 days, to follow one another by one day in nearly the same orbital track. Thus, a point on the surface was imaged by one satellite (ERS-1) on a given day and by the other satellite (ERS-2) on the following day. In the case where tandem data are not available or not appropriate for DEM generation, deformation rates should be estimated independently and removed from the interferograms used for DEM production.

III. Posteruption DEM: TOPSAR DEM Processing

The NASA–JPL airborne SAR (AIRSAR)–TOPSAR system is a left-looking two-antenna InSAR system onboard a NASA DC-8 aircraft. The baseline of the two antennas is 2.5 m, oriented about 27.2° from the vertical [15], [32]. The normal altitude of the aircraft is about 9 km, and the radar look angles range between 30° and 55° from the vertical. Because the two interferometric images are acquired simultaneously, atmospheric and deformation effects do not play a role in TOPSAR DEM generation. The TOPSAR data presented here were collected at C-band (wavelength of 5.7 cm) operating with a 40-MHz range bandwidth. The image swath width on the ground in the range direction is about 10 km, and the slant range resolution is about 3.3 m. The derived DEM has a pixel spacing of 5 m and a random rms height error of about 3 m due to the phase noise [15], [32].

Ten flight passes were made over the Okmok volcano during the 2000 Pacific Rim Campaign (*http://airsar.jpl.nasa.gov*). We have obtained ten DEMs, each of which corresponds to an individual flight pass, from JPL processed with the AIRSAR–TOPSAR Integrated Processor (version 6.10). Flight heading angles are 53° for four passes, 233° for three passes, 324° for two passes, and 144° for one pass. A DEM mosaic was produced based on metadata provided in each DEM file. Visual checks suggest that height offsets between two DEMs with overlap are far greater than the specified vertical accuracy of about 3 m. Hence, geometric correction procedures are needed to render a DEM mosaic with vertical accuracy consistent with the TOPSAR specification (Fig. 2).

To remove the horizontal and vertical misalignments between different TOPSAR passes, we used the "multimatch-multimosaic" program suite implemented by JPL [33]. Cross correlations are performed between each pair of TOPSAR passes with

overlap to determine the (X, Y, Z) offsets at a number of locations. Then a three-dimensional (3-D) affine transformation for each of the DEMs is calculated that best fits all of the measured offsets (Fig. 2). Treating each pixel in a DEM as a 3-D vector, the following affine transformation is used to convert the input vector I into a output vector O [33]

$$
\begin{aligned}
O &= MI + T \\
M &= \begin{bmatrix} Lx & 0 & 0 \\ 0 & Ly & 0 \\ 0 & 0 & Lz \end{bmatrix} + Qx \begin{bmatrix} 0 & 0 & 0 \\ 0 & 0 & -1 \\ 0 & 1 & 0 \end{bmatrix} \\
&\quad + Qy \begin{bmatrix} 0 & 0 & 1 \\ 0 & 0 & 0 \\ -1 & 0 & 0 \end{bmatrix} + Qz \begin{bmatrix} 0 & -1 & 0 \\ -1 & 0 & 0 \\ 0 & 0 & 0 \end{bmatrix} \\
&\quad + Kx \begin{bmatrix} 0 & 0 & 0 \\ 0 & 0 & 0 \\ 0 & 1 & 0 \end{bmatrix} + Ky \begin{bmatrix} 0 & 0 & 0 \\ 0 & 0 & 0 \\ 1 & 0 & 0 \end{bmatrix} + Kz \begin{bmatrix} 0 & 0 & 0 \\ 1 & 0 & 0 \\ 0 & 0 & 0 \end{bmatrix} \\
T &= [Tx \quad Ty \quad Tz]^T
\end{aligned} \tag{1}
$$

where M is the transformation matrix; Lx, Ly, and Lz are scale factors in x, y, and z directions; Qx, Qy, and Qz are the factors of rotation about the x, y, and z axes; Kx, Ky, and Kz are the skews about the x, y, and z axes; and T is the translation vector with its components Tx, Ty, and Tz. The offset estimations, used for calculating the 3-D affine transformation matrix M and the translation vector T, are obtained by cross-correlation technique based on either the radar amplitude images or the corresponding DEM elevation images. It is recommended that amplitude images be used for parallel and antiparallel passes, and DEM images be used for scenes that cross at any other angle [34].

For the ten TOPSAR passes over the Okmok volcano, we produced 19 sets of offset estimates. These offsets were filtered to remove outliers. We find that most horizontal offsets between different passes are less than 15 m. However, one particular scene is offset from others by about 50 m. The TOPSAR DEM mosaic, refined with the 3-D affine transformation technique, is shown in Fig. 3.

Fig. 4(a) is a height difference image produced by subtracting a TOPSAR DEM mosaics produced without the affine adjustment from one produced with the adjustment. A profile across this image is shown in Fig. 4(b). Height differences across the whole image range from about -45 to 49 m with standard deviation of 7.5 m. The differences are caused by both translational and rotational misalignments between individual DEMs used to produce the unadjusted DEM mosaic. The geolocation of the TOPSAR DEM mosaic is then improved by correlating both the TOPSAR DEM image with the existing U.S. Geological Survey (USGS) DEM [20] and the radar amplitude image with the Landsat-7 image (Fig. 1). The geolocation of the final TOPSAR DEM is accurate to within one pixel of the Landsat-7 image (Fig. 1), which has a specified geolocation accuracy of ± 10 m.

IV. Preeruption DEM: ERS InSAR DEM Processing

In order to produce high-accuracy DEMs using repeat-pass ERS-1 and ERS-2 SAR images, atmospheric anomalies need

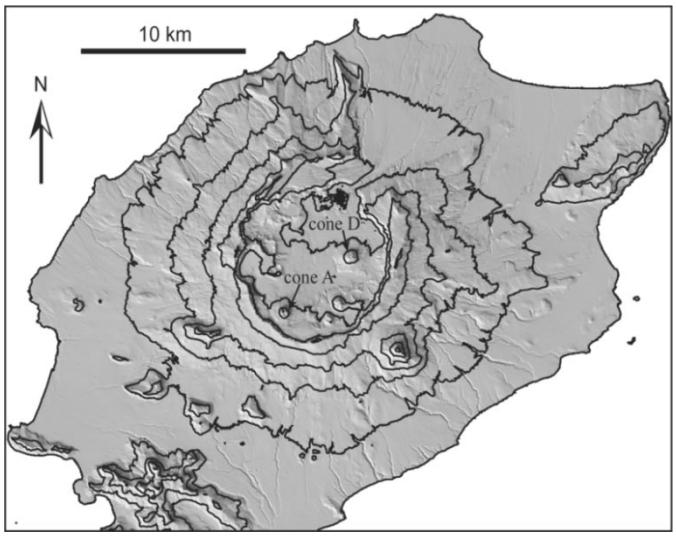

Fig. 3. Posteruption DEM over the Okmok volcano, Alaska using TOPSAR DEMs. A 3-D affine transformation is applied to correct geometric misalignments between different passes with overlap. The DEM contour interval is 200 m.

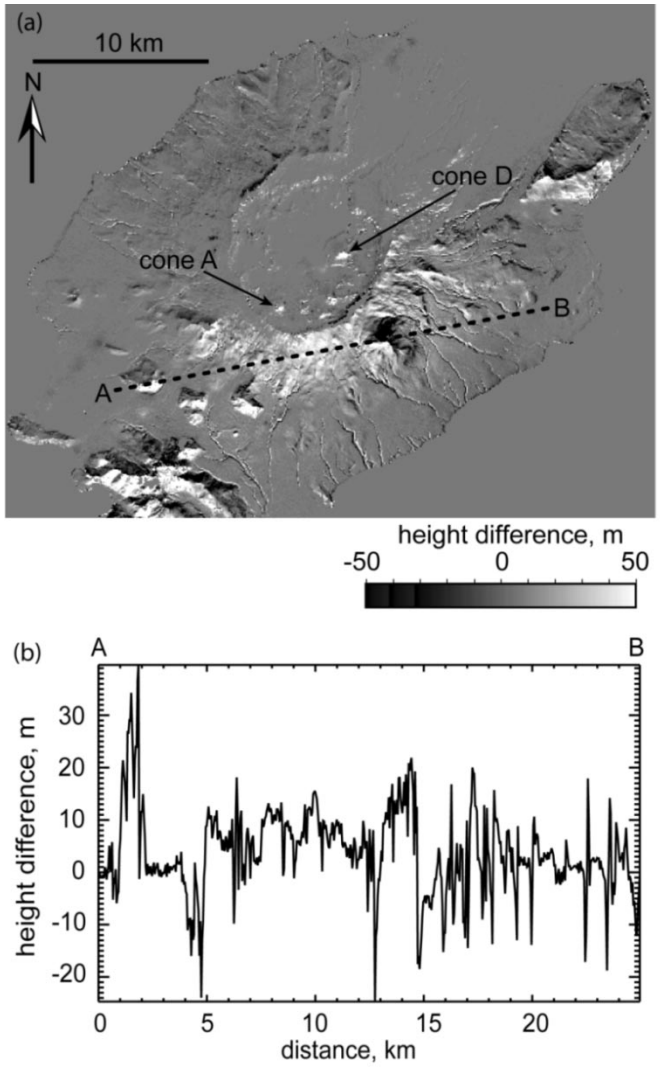

Fig. 4. (a) Difference between two DEM mosaics produced with and without the affine correction. (b) Height difference along a profile from A to B. Height difference is due to the misalignment in the DEM mosaic without affine rectification.

TABLE I
INTERFEROMETRIC DATA ACQUISITION PARAMETERS

Orbit 1	Orbit 2	Date 1	Date 2	Bn (m)
E1_22376	E2_02703	19951025	19950126	83
E1_10781	E1_11282	19930807	19930911	403
E1_11783	E1_12284	19931016	19931120	395
E1_11010	E1_11511	19930823	19930927	690

to be carefully considered because images used for InSAR processing are acquired at different times. Also, a compromise between baseline and interferometric coherence has to be made to select InSAR pairs suitable for DEM generation. Finally, for tectonically or volcanically active regions, any deformation signal must be removed from the interferograms used for DEM generation (Fig. 2).

Among the available ERS SAR images acquired before the 1997 eruption, four pairs were selected for DEM generation (Table I). In general, interferometric coherence is maintained reasonably well within the caldera and it is lost around the caldera rim where terrain is rugged and persistent snow patches are present. This is sufficient as we only need to determine a preeruption DEM within the caldera floor, part of which is covered by the new lava from the 1997 eruption. The caldera floor subsided about 1.4 m during the April 1997 eruption, and inflated at about 10 cm/year after the eruption [19]–[21]. Therefore, over areas that are not covered by 1997 lava flows, the topographic change between 1993 (or 1995) and 2000 is about 1.1 m (1.4-m subsidence between the summers of 1995 and 1997, and about 10-cm/year inflation from 1997 and 2000) at maximum.

We first estimate the volcanic inflation during the time periods of the interferograms used for DEM generation, and remove the deformation signal from these interferograms (Table I). Ground surface deformation associated with the 1997 eruption at Okmok volcano has been systematically studied with InSAR [19]–[21]. The reported preeruptive inflation is larger than 14 mm/month during October 31, 1992 and November 20, 1993, and about 4 mm/month during the summers of 1993 and 1995 [20], [21]. In addition to the images shown in Lu *et al.* [20], we produced several more image pairs with small baselines as well as short time separation (Fig. 5). The first interferogram spans 70 days from June 14 to August 23, 1993, with the perpendicular component of baseline, B_n, equal to 32 m [Fig. 5(a)]. The second interferogram covers the 35-day time interval from September 11 to October 16, 1993 with $B_n = 25$ m [Fig. 5(b)]. The third interferogram spans the 105-day time window between May 22, and September 4, 1995 with $B_n = 22$ m [Fig. 5(c)]. Because these interferograms (Fig. 5) have very small baselines, they are insensitive to DEM errors. Therefore, we can use either the posteruption TOPSAR DEM (Fig. 3) or the preexisting USGS DEM [20] to remove topographic effects for deformation analysis. Because these interferograms have shorter time separation and are temporally close to the interferograms used for DEM generation, they better depict the deformation that occurred in the interferograms used for DEM generation (Table I) than those shown by Lu *et al.* [20].

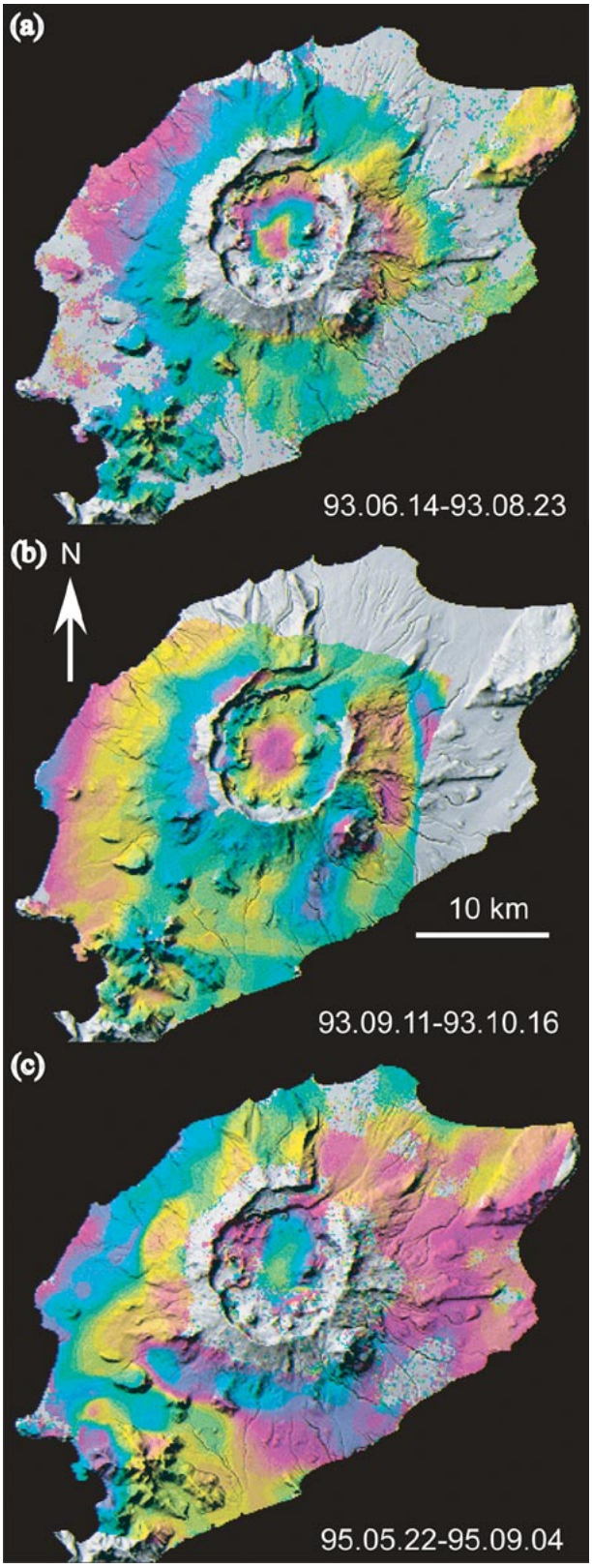

Fig. 5. Deformation interferograms during different time periods. The inflation was calculated and removed from those interferograms used for DEM generation. A full cycle of colors represents 28.3-mm surface deformation along the satellite look direction. Areas of coherence loss are uncolored.

To remove the deformation from the DEM interferograms (Table I), we estimate the location and magnitude of the infla-

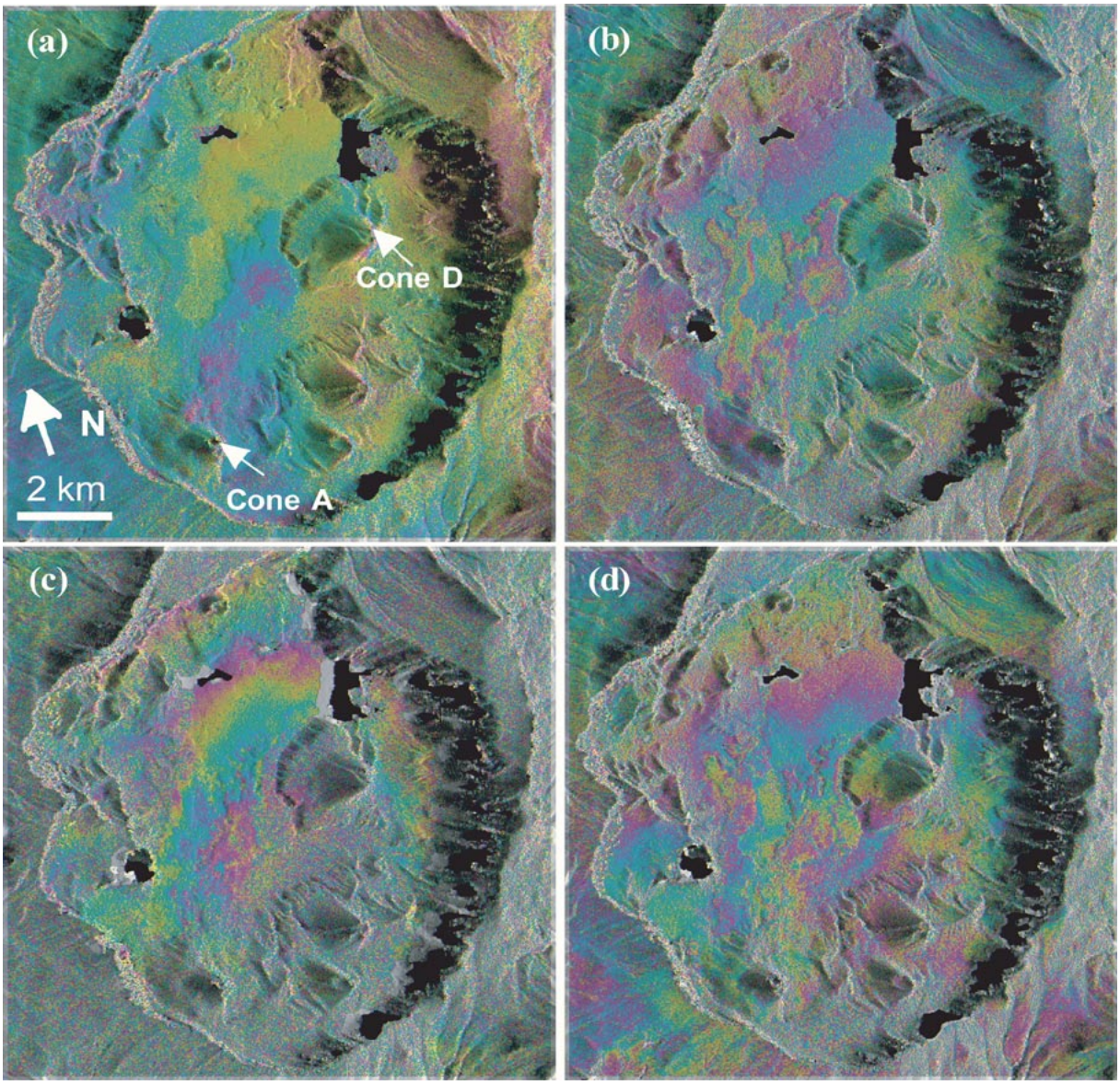

Fig. 6. Residual interferograms produced by subtracting the topographic phase from the original interferograms (Table I). (a) The tandem interferogram with $B_n = 83$ m and the TOPSAR DEM is used to remove the topographic phase. (b) The interferogram with $B_n = 403$ m and the TOPSAR DEM is used to remove the topographic phase. (c) The interferogram with $B_n = 395$ m and the DEM produced from the interferogram with $B_n = 403$ m is used to remove the topographic phase. (d) The interferogram with $B_n = 690$ m and the DEM produced from the interferogram with $B_n = 403$ m is used to remove the topographic phase. A full cycle of colors represents a phase change of 360°.

tion source responsible for the surface deformation using a point source embedded in an elastic homogeneous half-space [35]. We interpret this source to represent a magma chamber at depth. Deformation predicted by the best fitting model is removed from the DEM interferograms (Table I). We conclude that the magma body is located over the center of the caldera at about 3 km deep, and the maximum inflation is about 18 and 4 mm per 35 days during the summers of 1993 and 1995, respectively. The depth and location of the magma sources are quite compatible with the results obtained previously [19]–[21]. The error in deformation estimation will transfer into error in the DEM [13]

$$\Delta Z = \frac{4\pi}{\lambda}\frac{H\tan\theta}{B_n}\Delta\phi \tag{2}$$

where ΔZ is the height error due to error in interferometric phase, $\Delta\varphi$; λ is SAR wavelength (5.7 cm); B_n is the perpendicular baseline; H is SAR altitude, and is about 790 km; and θ is the SAR look angle which is about 22.7° from the vertical.

We estimate the uncertainty of the estimated deformation during the summer of 1993 is about 4 mm per 35 days, which corresponds to interferometric phase value of 0.9 rad. This error will propagate into error of about 3 m in the preeruption DEM elevation with a broad spatial wavelength.

The baseline vectors for all the interferograms are calculated using PRC vectors from D-PAF [23]. These baseline vectors are further refined using the posteruption DEM from the above-mentioned TOPSAR data based on the approach described by Rosen *et al.* [24] and ground points with known elevation from the TOPSAR DEM mosaic (Fig. 3). About 100 points are selected, and all of them lie within the caldera but far away from the 1997 lava flows. We use a least-squares approach to estimate

the baseline components, and all ground points are weighted equally.

An unwrapped interferometric phase image together with the precision baseline and imaging geometry are needed to derive the topographic heights [11], [36], [37]. The following hierarchical approach, similar to the one proposed by Lanari *et al.* [38], is used to facilitate the phase unwrapping procedure [39], [40]. We start with the interferogram with smallest baseline (i.e., the tandem pair acquired on October 25 and 26, 1995). We first subtract the topographic phase from the interferogram using the TOPSAR DEM. The residual fringes are unwrapped [Fig. 6(a)], and the topographic phase is added back to this result. A DEM based on this tandem interferogram is then produced. Next, we unwrap the August–September 1993 interferogram with $B_n = 403$ m (Table I), because the coherence for this interferogram is better than the October–November 1993 pair (with $B_n = 395$ m) (Table I). The simulated topographic phase based on the TOPSAR DEM is removed from the interferogram. The resulting residual interferogram is unwrapped [40] [Fig. 6(b)], and a DEM is generated. Note that we did not use the DEM from the tandem interferogram to simulate the topographic phase, because the TOPSAR DEM is far more accurate than the DEM based on the tandem pair. The tandem DEM is produced from an interferogram with a small baseline. Consequently, the interferometric phase is not very sensitive to topographic relief and any possible atmospheric delay anomalies in the data will significantly bias the DEM accuracy. However, if an existing DEM is not available, the DEM produced using the interferogram with smaller baseline can be used to simulate the topographic phase in the interferogram with larger baseline. Finally, the DEM produced using the interferogram with $B_n = 403$ m [Fig. 6(b)] is then used to assist unwrapping the October–November 1993 pair (with $B_n = 395$ m) [Fig. 6(c)] and the interferogram with $B_n = 690$ m [Fig. 6(d)]. Two more DEMs are produced.

A simple weighted approach is used to combine the four DEMs

$$h = \frac{\sum_{i=1}^{4} h_i c_i B_i^2}{\sum_{i=1}^{4} c_i B_i^2} \tag{3}$$

where h_i and c_i are height and coherence values from the four DEMs, and B_i is the perpendicular component of the baseline for each interferogram. The height value of each pixel in the final DEM results from the weighted average of the four DEMs, and height from the interferogram with larger baseline and higher coherence will be weighed more. This procedure not only reduces the possible atmosphere-induced errors in each DEM but also improves accuracy of the final DEM. We use this procedure to generate a DEM depicting the topography of Okmok volcano before the 1997 eruption.

V. Eruption Volume Estimation

Now that we have a preeruption DEM and a posteruption DEM, the flow volume is easy to calculate. Fig. 7 shows the thickness of the 1997 lava flows derived from the difference between the preeruption DEM (produced using ERS interferograms) and the posteruption DEM (produced using TOPSAR data). The DEM differences have been smoothed with a boxcar filter of width 100 m to reduce the random noise. The areal extent of the lava flow can be estimated by thresholding the lava thickness map (Fig. 7). Using the 5.0 m as a threshold, we estimate that the extent of the lava flows is about 9.8 km^2, which agrees well with that calculated from a Landsat-7 ETM+ image (9.47 km^2) (Fig. 1). The red line in Fig. 7 represents the lava flow margin based on field data that were collected in August 2001 [41]. Examining Fig. 7, we can see that the thickness of the lava is very heterogeneous. The thickest portion of the lava happens to be near the distal end (adjacent to Cone D) of the right arm of the Y-shaped flows, and reaches almost 50 m. The flow is thickest here because there was a substantial preexisting depression (as much as 15 m deep), which caused the flow pond. In fact, this depression hides the extreme thickness in this area (about 50 m) because the closest measurements of the flow margin's height do not exceed 20 m [41]. If the preeruption surface is not flat, therefore, measurements at the edges are not representative of total thickness. DEM data are then required to calculate more accurate values of lava thickness and eruption volume [5]–[7]. The lava near the eruptive vent (Cone A) is, on average, thinner than the rest, and can be as thin as a few meters as the underlying slope is quite steep near Cone A.

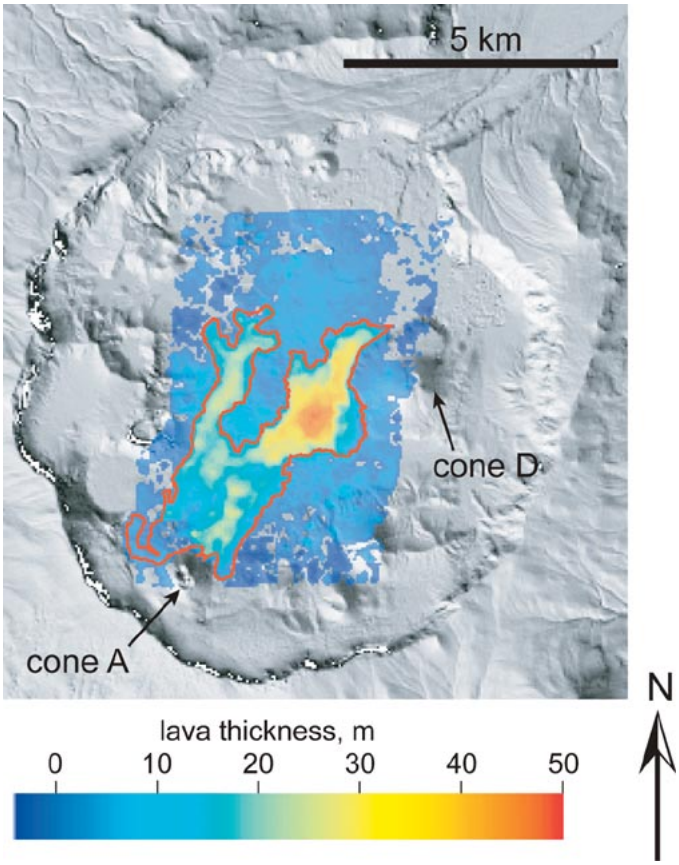

Fig. 7. Thickness of lava flows for the April 1997 eruption at Okmok volcano. The thickness is derived based on height difference between the preeruption and posteruption DEMs. The red line represents the lava perimeter based on field data that were collected in August 2001.

We calculate the bulk volume of the 1997 eruption to be 0.154 ± 0.025 km^3. To derive the dense-rock equivalent volume, it is needed to correct for void space in the erupted volume due to vesiculation. The 1997 lava flow is similar to Hawaiian aa lava, with vesicularity ranging from 25% to 75%. Therefore, the estimated dense-rock equivalent volume is about 0.07–0.14 km^3, which is comparable with those estimations based on surface deformation measurement (0.05–0.09 km^3) [20], [21].

The standard deviation of our measurement can be estimated using the rms values of DEM difference over the areas outside of the lava flows. We estimate the mean and standard deviation of the DEM difference to be 1.8 and 2.6 m, respectively, after the spatial smoothing with the 100-m boxcar filter. This means the DEM produced using the four ERS interferograms has a relative vertical accuracy of about 5.0 m at 95% confidence limit. The ERS SAR and TOPSAR systems both use C-band (5.7-cm wavelength) radar, so we expect the radar-derived elevation to have the same relationship to the true ground elevation. The Okmok lava flow is completely unvegetated so the InSAR elevation in this case will be a "bare-earth" elevation. Note that the procedure we used to produce the ERS combined DEM automatically corrected the ERS absolute location and other systematic errors from baseline uncertainty to match the adjusted TOPSAR DEM. Because the lava flow volume only depends on the difference between the two DEMs, the absolute geolocation of the DEMs is not important, only their coregistration.

VI. Conclusion

Accurate DEMs can be produced using InSAR techniques with multiple interferograms. Single-pass two-antenna InSAR systems, such as TOPSAR, are the best for DEM production because the simultaneous InSAR removes many error sources. Systematic TOPSAR processing errors that cause misalignment between different DEM patches can be corrected. Repeat-pass single-antenna InSAR systems are also capable of producing accurate DEMs but multiple interferograms are required to reduce errors due to atmospheric contributions and a reference DEM or ground control is necessary to refine baseline estimates and remove systematic errors. We estimate the eruption volume and lava thickness for the 1997 eruption at Okmok volcano, by using TOPSAR data to produce a posteruption DEM and ERS InSAR imagery to generate a preeruption DEM. The InSAR calculation of the flow volume is substantially more accurate and precise than that achievable by using field-based lava thickness measurements.

Acknowledgment

The authors thank the ASF for providing ERS-1/ERS-2 SAR data; the JPL AIRSAR Group for the TOPSAR data; E. O'Leary, S. Shaffer, E. Chapin, and S. Hensley for help on working with TOPSAR data and with the multimatch-multimosaic software; C. Werner for help on phase unwrapping; D. Gesch and T. Masterlark for technical reviews and comments; R. Rykhus, T. Masterlark, and B. Wylie for assistance on working with the lava perimeter GIS data layer and figures; S. Rowland, J. Freymueller, and C. Werner for their constructive comments. The authors are particularly grateful to the 65 detailed comments by S. Rowland.

References

[1] G. Wadge, "The storage and release of magma on Mount Etna," *J. Volcanol. Geotherm. Res.*, vol. 2, pp. 361–384, 1977.
[2] J. A. Crisp, "Rates of magma emplacement and volcanic output," *J. Volcanol. Geotherm. Res.*, vol. 20, pp. 177–201, 1984.
[3] J. J. Dvorak and D. Dzurisin, "Variations in magma supply rate at Kilauea volcano, Hawaii," *J. Geophys. Res.*, vol. 98, pp. 255–268, 1993.
[4] S. K. Rowland, M. E. MacKay, H. Garbeil, and P. J. Mouginis-Mark, "Topographic analyses of Kilauea volcano, Hawaii, from interferometric airborne radar," *Bull. Volcanol.*, vol. 61, pp. 1–14, 1999.
[5] J. B. Murray, "High-level magma transport at Mount Etna volcano, as deduced from ground deformation measurements," in *Magma Transport and Storage*, M. P. Ryan, Ed. London, U.K.: Wiley, 1990, pp. 357–383.
[6] J. B. Murray and N. F. Stevens, "New formulae for estimating lava flow volumes at Mt. Etna volcano Sicily," *Bull. Volcanol.*, vol. 61, pp. 515–526, 2000.
[7] N. F. Stevens, G. Wadge, and J. B. Murray, "Lava flow volume and morphology from digitized contour maps: A case study at Mount Etna, Sicily," *Geomorphology*, vol. 28, pp. 251–261, 1999.
[8] C. W. Molander, "Photogrammetry," in *Digital Elevation Model Technologies and Applications: The DEM Users Manual*, D. F. Maune, Ed. Bethesda, MD: Amer. Soc. Photogrammetry and Remote Sensing, 2001, pp. 121–142.
[9] R. Fowler, "Topographic Lidar," in *Digital Elevation Model Technologies and Applications: The DEM Users Manual*, D. F. Maune, Ed. Bethesda, MD: Amer. Soc. Photogrammetry and Remote Sensing, 2001, pp. 207–26.
[10] R. Bürgmann, P. A. Rosen, and E. J. Fielding, "Synthetic aperture radar interferometry to measure Earth's surface topography and its deformation," *Ann. Rev. Earth Planet. Sci.*, vol. 28, pp. 169–209, 2000.
[11] S. Hensley, R. Munjy, and P. Rosen, "Interferometric synthetic aperture radar (IFSAR)," in *Digital Elevation Model Technologies and Applications: The DEM Users Manual*, D. F. Maune, Ed. Bethesda, MD: Amer. Soc. Photogrammetry and Remote Sensing, 2001, pp. 143–206.
[12] D. Massonnet and K. Feigl, "Radar interferometry and its application to changes in the Earth's surface," *Rev. Geophys.*, vol. 36, pp. 441–500, 1998.
[13] P. A. Rosen *et al.*, "Synthetic aperture radar interferometry," *Proc. IEEE*, vol. 88, pp. 333–380, 2000.
[14] H. Zebker *et al.*, "Remote sensing of volcano surface and internal processing using radar interferometry," in *Remote Sensing of Active Volcanism*. ser. , AGU Monograph, P. Mougins-Mark *et al.*, Eds. Washington, DC: AGU, 2000, pp. 179–205.
[15] H. Zebker *et al.*, "The TOPSAR interferometric radar topographic mapping instrument," *IEEE Trans. Geosci. Remote Sensing*, vol. 30, pp. 933–940, Sept. 1992.
[16] T. G. Farr and M. Kobrick, "Shuttle Radar Topography Mission produces a wealth of data," *EOS Trans.*, vol. 81, pp. 583–585, 2000.
[17] A. L. Gray and P. J. Farris-Manning, "Repeat-pass interferometry with airborne synthetic aperture radar," *IEEE Trans. Geosci. Remote Sensing*, vol. 31, pp. 180–191, Jan. 1993.
[18] T. P. Miller, R. G. McGimsey, D. H. Richter, J. R. Riehle, C. J. Nye, M. E. Yount, and J. A. Dumoulin, "Catalog of the Historically Active Volcanoes of Alaska," USGS, Sioux Falls, SD, Tech. Rep. 98–582, 1998.
[19] Z. Lu, D. Mann, and J. Freymueller, "Satellite radar interferometry measures deformation at Okmok volcano," *EOS Trans.*, vol. 79, no. 39, pp. 461–468, 1998.
[20] Z. Lu, D. Mann, J. Freymueller, and D. Meyer, "Synthetic aperture radar interferometry of Okmok volcano, Alaska: Radar observations," *J. Geophys. Res.*, vol. 105, pp. 10 791–10 806, 2000.
[21] D. Mann, J. Freymueller, and Z. Lu, "Deformation associated with the 1997 eruption of Okmok volcano, Alaska," *J. Geophys. Res.*, vol. 107, no. B4, 2002.
[22] E. Sansosti, R. Lanari, G. Fornaro, G. Franceschetti, M. Tesauro, G. Puglisi, and M. Coltelli, "Digital elevation model generation using ascending and descending ERS-1/ERS-2 tandem data," *Int. J. Remote Sens.*, vol. 20, pp. 1527–1547, 1999.
[23] F. H. Massmann, "Information for ERS PRL/PRC users," GeoForschungsZentrum Potsdam, Potsdam, Gemany, Tech. Note, 1995.
[24] P. Rosen, S. Hensley, H. Zebker, F. H. Webb, and E. J. Fielding, "Surface deformation and coherence measurements of Kilauea volcano, Hawaii, from SIR-C radar interferometry," *J. Geophys. Res.*, vol. 101, pp. 23 109–23 125, 1996.

[25] H. A. Zebker and J. Villasenor, "Decorrelation in interferometric radar echoes," *IEEE Trans. Geosci. Remote Sensing*, vol. 30, pp. 950–959, Sept. 1992.
[26] F. Gatelli *et al.*, "The wavenumber shift in SAR interferometry," *IEEE Trans. Geosci. Remote Sensing*, vol. 32, pp. 855–865, July 1994.
[27] A. M. Guarnieri, G. Fornaro, and F. Rocca, "Interferometric SAR quality enhancing by space-varying spectral shift pre-filtering," in *Proc. ERS-Envisat Symp.*, vol. SP-461, Gothenburg, Sweden, 2000.
[28] E. Rodriguez and J. Martin, "Theory and design of interferometric synthetic aperture radars," *Proc. Inst. Elect. Eng.*, vol. 139, pp. 147–159, 1992.
[29] H. Zebker, P. Rosen, and S. Hensley, "Atmospheric effects in interferometric synthetic aperture radar surface deformation and topographic maps," *J. Geophys. Res.*, vol. 102, pp. 7547–7563, 1997.
[30] R. Goldstein, "Atmospheric limitations to repeat-track radar interferometry," *Geophys. Res. Lett.*, vol. 22, pp. 2517–2520, 1997.
[31] N. F. Stevens, G. Wadge, and C. A. Williams, "Post-emplacement lava subsidence and the accuracy of ERS InSAR digital elevation models of volcanoes," *Int. J. Remote Sens.*, vol. 22, pp. 819–828, 2001.
[32] S. Madsen, J. Martin, and H. Zebker, "Analysis and evaluation of the NASA/JPL TOPSAR across-track interferometric SAR system," *IEEE Trans. Geosci. Remote Sensing*, vol. 33, pp. 383–391, Mar. 1995.
[33] S. Hensley and S. Shaffer, "DEM mosaicking," in *UCLA Extension Class Notes for Synthetic Aperture Radar Interferometry*, 1996.
[34] E. Chapin, "Users guide for Multimosaic: Version 1.1," JPL, Pasadena, CA, 334-97-004, 2000.
[35] K. Mogi, "Relations between the eruptions of various volcanoes and the deformations of the ground surface around them," *Bull. Earthquake Res. Inst. Univ. Tokyo*, vol. 36, pp. 99–134, 1958.
[36] S. Madsen, H. Zebker, and J. Martin, "Topographic mapping using radar interferometry: Processing techniques," *IEEE Trans. Geosci. Remote Sensing*, vol. 31, pp. 246–256, Jan. 1993.
[37] D. Small, C. Werner, and D. Muesch, "Geocoding and validation of ERS-1 InSAR-derived digital elevation models," *ERSSeL Adv. Remote Sens.*, vol. 4, pp. 26–39, 1995.
[38] R. Lanari *et al.*, "Generation of digital elevation models by using SIR-C/X-SAR multifrequency two-pass interferometry: The Etna case study," *IEEE Trans. Geosci. Remote Sensing*, vol. 34, pp. 1097–1114, Sept. 1996.
[39] R. Goldstein, H. Zebker, and C. Werner, "Satellite radar interferometry: Two-dimensional phase unwrapping," *Radio Sci.*, vol. 23, pp. 713–720, 1988.
[40] M. Costantini, "A novel phase unwrapping method based on network programming," *IEEE Trans. Geosci. Remote Sensing*, vol. 36, pp. 813–821, May 1998.
[41] L. Moxey *et al.*, "The 1997 eruption of Okmok volcano, Alaska, a synthesis of remotely sensed data," *EOS Trans.*, vol. 82, p. 47, 2001.

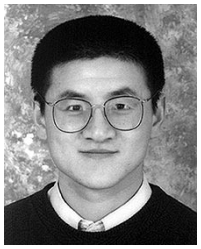

Zhong Lu (S'96–A'97–M'97) received the M.S. degree from Beijing University, Beijing, China, in 1992, and the Ph.D. degree from the University of Alaska, Fairbanks, in 1996.

Since February 1997, he has been conducting research at the U.S. Geological Survey EROS Data Center (EDC), Sioux Falls, SD. He is currently the Project Lead of synthetic aperture radar and interferometric SAR applications. He is a Principal Investigator for the National Aeronautics and Space Administration, Washington, DC, the European Space Agency, Frascati, Italy, the National Space Development Agency of Japan, Tokyo, Japan, and the German Aerospace Center (DLR), Oberpfaffenhofen, Germany, to study volcanoes using Radarsat, ERS-1, ERS-2, Envisat, JERS-1, ALOS satellite SAR imagery, and SRTM data. He has worked with satellite SAR imagery for nine years. His research interests include technique development and applications of SAR and InSAR, with an emphasis on studying the surface deformation associated with volcanic, seismic, and hydrological processes.

Dr. Lu is the recipient of the 2001 Raytheon Distinguished Level Award for Excellence in Technology, and the 1999 Jerald J. Cook Memorial Award. He is a member of American Geophysical Union (AGU).

Eric Fielding received the A.B. degree from Dartmouth College, Hanover, NH, in 1982, and the Ph.D. degree from Cornell University, Ithaca, NY, in 1989.

He is currently a Research Scientist with t the Jet Propulsion Lab, Caltech, Pasadena, CA. He has been using digital topographic data for more than 15 years and satellite imagery for 20 years to study geology, especially active faults in many locations worldwide.

Matthew R. Patrick received the B.S. degree from Cornell University, Ithaca, NY, in 1999, and the M.S. degree in geology from the University of Alaska, Fairbanks, in 2002. He is currently pursuing the Ph.D. degree at the University of Hawaii, Manoa.

His past work addressed lava flow cooling and its comparison with thermal infrared imagery. Current work involves ground-based thermal monitoring of Strombolian activity.

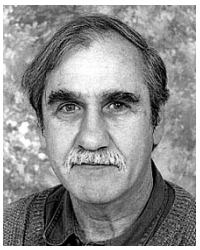

Charles M. Trautwein received the P.Eng. degree, in 1963, and the Geol.Eng. degree, in 1969, both from the Colorado School of Mines, Golden.

He currently manages the Land Remote Sensing Applications Project at the U.S. Geological Survey's Earth Resources Observation Systems Data Center, Sioux Falls, SD. Since 1975, he has been engaged in fundamental and applied remote sensing research with special emphasis on land surface processes and applications in mineral resource investigations.